1 Preprint of:

2 Last century warming over the Canadian Atlantic shelves linked to weak
3 Atlantic Meridional Overturning Circulation

4

5

6 **Authors**

7 B. Thibodeau[1,2][†][*], C. Not[1,2][†], J. Zhu[3], A. Schmittner[4], D. Noone[4], C. Tabor[5], J. Zhang[6], Z. Liu[7]

8

9 **Affiliations**

10 [1]Department of Earth Sciences, The University of Hong Kong, Hong Kong SAR

11 [2]The Swire Institute of Marine Science, The University of Hong Kong, Hong Kong SAR

12 [3]Department of Earth and Environmental Sciences, University of Michigan, United-States of
13 America

14 [4]College of Earth, Ocean, and Atmospheric Sciences, Oregon State University, United-States
15 of America

16 [5]Center for Integrative Geosciences, University of Connecticut, United-States of America

17 [6]CCS-2 and CNLS, Los Alamos National Laboratory, Los Alamos, New Mexico, United-
18 States of America

19 [7]Atmospheric Science Program, Department of Geography, The Ohio State University, United-
20 States of America

21

22 *Correspondence to: bthib@hku.hk

23 † Equal contribution

24
25

26 **Abstract**

27 The Atlantic meridional overturning circulation (AMOC) is a key component of the global

28 climate system. Recent studies suggested a 20th-century weakening of the AMOC of

29 unprecedented amplitude ($\sim$ 15%) over the last millennium. Here, we present a record of $\delta^{18}O$

30 in benthic foraminifera from sediment cores retrieved from the Laurentian Channel and

31 demonstrate that the $\delta^{18}O$ trend is linked to the strength of the AMOC. In this 100-year record,

32 the AMOC signal decreased steadily to reach its minimum value in the late 1970's, where the

33 weakest AMOC signal then remains constant until 2000. We also present a longer $\delta^{18}O$ record

34 of 1,500 years and highlight the uniqueness of the last century $\delta^{18}O$ trend. Moreover, the Little

35 Ice Age period is characterized by statistically heavier $\delta^{18}O$, suggesting a relatively weak

36 AMOC. Implications for understanding the mechanisms driving the intensity of AMOC under

37 global warming and high-latitude freshwater input are discussed.

38

39   **1. Introduction**

40   The Atlantic meridional overturning circulation (AMOC) encompasses the advection
41   of warm and saline waters in the upper ocean to the northern parts of the Atlantic, where it
42   cools, becomes denser and sinks, ultimately creating North Atlantic deep water. Both
43   observational and modeling studies have suggested that the strength of this oceanic circulation
44   cell is not constant through time (Bohm et al., 2015; Rahmstorf et al., 2015), and that these
45   changes drive many other climatic events across wide ranges of spatial and temporal scales
46   (Delworth et al., 2008). Weakening of the AMOC as a response to warming and/or high latitude
47   freshwater release is a common feature of many climate models (Bakker et al., 2016; Jungclaus
48   et al., 2006; Krebs & Timmermann, 2007; Stouffer et al., 2006; Yang et al., 2016; Yu et al.,
49   2016). However, a recent study suggested that current models are not sensitive enough in their
50   AMOC response (Liu et al., 2017), which implies that previous model projections of collapse
51   probabilities are underestimated. The possibility of an AMOC collapse under global warming
52   is a major concern due to its potentially dramatic impacts on oceanic circulation and global
53   climate. The consequences of freshwater input near sites of deep water formation are a
54   contemporary concern as the total freshwater storage of the North Atlantic increased by 19 000
55   km^3 between 1961 and 1995 (~0.02 Sv on average; Curry, 2005). This freshwater is transported
56   to the Labrador Sea and creates salinity anomalies (Luo et al., 2016). It is therefore increasingly
57   critical that we understand the impacts of climate change and freshwater release on convection
58   in the Labrador Sea and its corresponding impact on AMOC intensity (Gregory et al., 2005).
59   This is especially true if we are to identify the forcing(s) responsible for the ongoing AMOC
60   weakening (Bakker et al., 2016; Thornalley et al., 2018).

61   High-resolution modeling (~10 km ocean, ~50 km atmosphere) suggests a robust
62   relationship between a weakening AMOC and the decrease in the proportion of Labrador-
63   derived water (Labrador Subarctic Slope Water : LSSW) entering the Northwest Atlantic shelf
64   compared to Atlantic-derived water (Atlantic Temperate Slope Water : ATSW) under climate
65   change (Saba et al., 2016). Interestingly, historical instrumental temperature data suggest a
66   significant reorganisation of the Northwest Atlantic slope currents from the bottom water of
67   the St. Lawrence Estuary (Gilbert et al., 2005). The significant bottom water warming (+1.7°C)
68   during the twentieth-century was attributed to a decrease in the proportion (72 to 53%) of cool
69   LSSW entering the Laurentian Channel (Gilbert et al., 2005). This warming was suggested to
70   be unique over the last millennium (Thibodeau et al., 2010a) and the last ~6,000 years
71   (Thibodeau et al., 2013). This major change in the regional oceanography has severe

72   environmental consequence, as the ATSW is characterized by lower dissolved oxygen content

73   than the LSSW which, in conjunction with localized eutrophication, is thought to be

74   responsible for the development of the permanent hypoxic zone in the St. Lawrence Estuary

75   (Benoit et al., 2006; Gilbert et al., 2005; Lefort et al., 2012; Thibodeau et al., 2006; Thibodeau

76   et al., 2010b). As detailed in figure 1, the recirculation gyre is considered to be controlled by

77   the strength of the formation of deep water in the Labrador Sea and thus by the strength of the

78   deep western boundary current (DWBC) (Zhang et al., 2007). A strong recirculation gyre keeps

79   the Gulf Stream path well separated from the coast (Fig 1a) and allows for southern penetration

80   of the LSSW. In episodes of weak convection characteristic of modern conditions (Rahmstorf

81   et al., 2015), a larger proportion of the warm water from the Gulf Stream and ATSW is

82   expected to be found in the Laurentian Channel bottom water (Fig 1b). It was further suggested

83   that the westward transport of Labrador current water along the continental shelf edge to the

84   south of the Grand Banks of Newfoundland could significantly contribute to temperature and

85   salinity variability from the Gulf of St Lawrence to the Gulf of Maine (Petrie & Drinkwater,

86   1993). The contribution of AMOC and its component currents on regional temperature changes

87   has led to the usage of ocean temperature as a surrogate for the AMOC intensities (e.g., the

88   AMOC index; Rahmstorf et al., 2015), which has been later confirmed by high-resolution

89   models (Saba et al., 2016). Moreover, a linear relationship was observed between the AMOC

90   intensity and the AMOC index using the CMIP5 climate model ensemble (Caesar et al., 2018).

91   Based on this relationship, it was estimated that AMOC intensity explains 89% of the variance

92   in the temperature-based AMOC index with other factor having a minor influence on the

93   observed temperature pattern (Caesar et al., 2018). Thus, the observed warming in the western

94   North Atlantic and consequently in the Laurentian Channel could be linked to the weakened

95   state of the AMOC (Caesar et al., 2018; Rahmstorf et al., 2015; Thornalley et al., 2018).

96   Here, we present two high-resolution records of oxygen isotope ($\delta^{18}O$) measurements

97   of the benthic foraminifera *Globobulimina auriculata* covering the last century and the last

98   1,500 years respectively. We demonstrate how these records can be used to track sub-surface

99   temperature of the western North Atlantic. We then tested this paleotemperature record against

100   instrumental measurements, new model simulations, AMOC index and other AMOC-related

101   proxies to link our record to the AMOC intensity. As such, we provide here one of the first

102   robust high-resolution reconstructions of the strength of the AMOC over the last 1,500 years

103   and highlight that the current AMOC is probably at its weakest state. While the uncertainties

104   are larger when we investigate older periods, we further report statistically heavier $\delta^{18}O$ during

105   the Little Ice Age (LIA), which is interpreted as weaker AMOC conditions during that time.

106   Thus, our record is significant for the investigation of the potential mechanisms responsible for

107   the last century AMOC weakening.

108

109   **2. Methods**

110   We investigated the effects of an AMOC reduction on the western North Atlantic

111   subsurface temperature via freshwater perturbation experiments using two climate models: the

112   University of Victoria climate model (UVic v2.9) and the water isotope-enabled Community

113   Earth System Model (iCESM1.3). The UVic model is a climate model of intermediate

114   complexity including an ocean general circulation model at coarse resolution ($3.6 \times 1.8°$, 19

115   vertical levels), a single-layer atmospheric energy-moisture balance model, a dynamic-

116   thermodynamic sea ice model, and biogeochemical components. The freshwater perturbation

117   experiment analyzed here has 0.05 Sv freshwater discharged into the North Atlantic between

118   45–65°N and 60–0°W for 100 years. Readers are referred to previous publications for a detailed

119   description of the experimental setup (Schmittner & Lund, 2015).

120   The water isotope-enabled Community Earth System Model version 1.3 (iCESM) is a

121   state-of-the-art fully coupled Earth system model with the capability to simulate the oxygen

122   isotopes in the hydrological cycle (Nusbaumer et al., 2017; Wong et al., 2017; Zhang et al.,

123   2017; Zhu et al., 2017a). The numerical experiments analyzed here are from a recent study

124   (Zhu et al., 2017b). The simulations were conducted with a horizontal resolution of $1.9 \times 2.5°$

125   (latitude × longitude) for the atmosphere and land, and a nominal 1° for the ocean and sea ice.

126   The ocean model consists of 60 uneven levels with an interval of ~10 m for the upper 200 m.

127   The preindustrial control simulation was run for 500 years, with forcing fixed at the values

128   from 1850 A.D., and water isotopes in the ocean initialized from the Goddard Institute for

129   Space Studies interpolated observational dataset (LeGrande & Schmidt, 2006). In the

130   freshwater perturbation experiment, 0.10 Sv of isotopically depleted fresh water was

131   discharged into the northern North Atlantic (50–70ºN) for 100 years. The $\delta^{18}O$ signature of the

132   freshwater forcing was set as −30 ‰ SMOW (Hillaire-Marcel & Causse, 1989). The simulation

133   of $\delta^{18}O$ in the model helps to test our interpretation of the benthic $\delta^{18}O$ records in the Laurentian

134   channel. The response of carbonate $\delta^{18}O$ (‰ PDB) to freshwater forcing is calculated in the

135   model with the simulated ocean temperature and $\delta^{18}O$ (‰ SMOW) of seawater, using the

136   paleotemperature equation of Shackleton (1974).

137   We then compiled $\delta^{18}O$ data (‰ VPDB) measured on the benthic foraminifera

138   *Globobulimina auriculata* in two sediment cores (CR02-23 and MD99-2220; core details in

139   S1-2) from the Laurentian Channel (Fig 1). The calcareous shells were picked under binocular

140   and roasted at ~ 200ºC for about 2 hours in order to eliminate organic matter. Samples were

141   analyzed with a Micromass Isoprime™ isotope ratio mass spectrometer in dual inlet mode

142   coupled to a MultiCarb™ preparation system. The CO_2 was extracted at 90ºC by acidification

143   with concentrated H_3PO_4. The analytical reproducibility determined by replicate measurements

144   of internal standard carbonate material was routinely better than 0.05 ‰, which is equivalent

145   to a precision of approximately 0.2°C..

146

147   **3. Results and Discussion**

148   *3.1. Modelled effect of reduced AMOC on subsurface temperature*

149   To test the link between AMOC strength and subsurface warming, the AMOC strength

150   was reduced in two models (iCESM and UVic) (see detailed results in S3). Both models used

151   here produced a large-scale subsurface warming in the northwest Atlantic at 45°N (Fig S1 and

152   S2) with a maximum of 1–3°C around 50°W. The AMOC reduction obtained with the UVic

153   model (~ 17 %) is consistent with the most recent estimate of weakening (Caesar et al., 2018;

154   Rahmstorf et al., 2015; Thornalley et al., 2018). This subsurface warming of the western North

155   Atlantic under weak AMOC conditions is expected from global gridded data set (Dima &

156   Lohmann, 2010), theory (Petrie & Drinkwater, 1993; Zhang, 2008; Zhang et al., 2007), coarse

157   (this study) as well as high-resolution and eddy-permitting models (Brickman et al., 2018;

158   Caesar et al., 2018; Saba et al., 2016; Thornalley et al., 2018). Thus, the warming can be

159   considered a robust fingerprint of the weakened AMOC. Moreover, the simulated water $\delta^{18}O$

160   is enriched by about 0.2–0.3‰ in the iCESM (Fig 2). This suggests a major increase in the

161   proportion of $\delta^{18}O$-enriched ATSW in the subsurface water, indicating a change in western

162   North Atlantic oceanography. This supports previous estimates based on temperature and

163   dissolved oxygen changes (Gilbert et al., 2005; Thibodeau et al., 2010a).

164

165   *3.2. Influence of temperature and water mass contribution on the $\delta^{18}O$ record*

166   Due to the strong stratification in the Laurentian Channel, the temperature variation at

167   our coring site reflects the temperature variation of the slope water entering the channel at

168 Cabot Strait (Gilbert et al., 2005). Thus, because of the high-sedimentation regime of this

169 region, our cores provide a unique proxy of the slope water with a resolution of about 2 years

170 per cm. It was demonstrated that isotopic signature of oxygen in *Globobulimina auriculata*

171 tests is a good proxy of temperature change in the Laurentian Channel over the last century

172 (Thibodeau, et al., 2010a). The warming instrumentally observed in the Laurentian Channel

173 bottom water seems well captured by *Globobulimina auriculata* $\delta^{18}O$ in the high sedimentation

174 box-core CR02-23 samples (Fig 3), as the $\delta^{18}O$ decreases from 1940 to 2000 by about 0.4 ‰

175 synchronously with the 2°C increase in temperature from the bottom water of the St. Lawrence

176 Estuary. However, the $\delta^{18}O$ of benthic foraminifera also records the change in the proportion

177 of water masses entering the Laurentian channel, as these water masses are characterized by

178 different isotopic conditions. Using the isotopic signature of both water mass (ATSW = 0.5 ‰

179 and LSSW = -0.5 ‰), it was estimated that the proportion of these water masses is currently

180 about 50-50 % (Thibodeau et al., 2010a). Based on dissolved oxygen and temperature, it was

181 hypothesized that the proportion of ATSW entering the Laurentian channel was much lower in

182 1940 at about 30% (Gilbert et al., 2005), which imply an increase of $\delta^{18}O$ by about 0.2 ‰

183 between 1940 and 2000. We observed that the $\delta^{18}O$ of seawater exhibits an enrichment of 0.2

184 to 0.3 ‰ in the subsurface western North Atlantic in the freshwater perturbation experiment

185 using iCESM (Fig 2), which is coherent with the magnitude of the increase in the proportion

186 of ATSW entering the Laurentian Channel inferred from temperature and dissolved oxygen

187 changes (Gilbert et al., 2005; Thibodeau et al., 2010a)). Considering a relationship of about -

188 0.22 ‰/°C (Ravelo & Hillaire-Marcel, 2007), one would expect a decrease of -0.44 ‰ in the

189 $\delta^{18}O$ of *Globobulimina auriculata* given the instrumentally-measured 2°C warming in the

190 bottom water between 1940 and 2000. The increase in seawater $\delta^{18}O$ of at least 0.2 ‰ (from

191 model and theory) combined to the expected decrease of about -0.44 ‰ due to higher

192 temperature should translate into a decrease of -0.24 ‰ in the benthic foraminifera calcite. In

193 our core, we observed a depletion of about 0.26 ‰ between the averaged pre-1940 values and

194 the post-2000 values, which likely support the notion that part of the temperature effect was

195 masked by the seawater $\delta^{18}O$ enrichment due to the change in water masses. While other

196 potential factors could influence the $\delta^{18}O$ locally (mixing event, diffusion) they do not seem to

197 be strong enough to mask the main signal driven by the AMOC as we demonstrated that 1) the

198 AMOC influences the temperature of the slope water (Section 3.1 and references therein), 2)

199 our site records these temperature variation (S4, Fig 3 and Gilbert et al., 2005) and 3) the $\delta^{18}O$

200 at our site records these temperature variation (section 3.2 and Thibodeau et al., 2010). We

201 therefore suggest that the Laurentian Channel benthic $\delta^{18}O$ record is strongly influenced by

202 AMOC intensity via the advection of the western North Atlantic subsurface temperature and
203 water mass dynamics.

204

205   *3.3. Comparison with other AMOC-related proxies over the last century*

206   An annually-resolved $\delta^{15}N$ record retrieved from soft corals over the Canadian shelf
207 shows a high degree of similarity with both the $\delta^{18}O$ record and the instrumental record of
208 temperature (Fig 3). This record was interpreted as an increase in the proportion of ATSW
209 reaching the Canadian shelf, a unique event of the last 1800 years (Sherwood et al., 2011) and
210 is consistent with the AMOC index (Caesar et al., 2018; Rahmstorf et al., 2015). The CR02-23
211 $\delta^{18}O$ record presented here is also in agreement with the AMOC index over the 1940-2000
212 period despite some leads and lags that can be attributed to either the different resolution and/or
213 time integration of the respective proxies. The leads and lags could also be caused by the fact
214 that the AMOC-index and our record integrate different signals; the AMOC-index estimates
215 the difference in the temperature anomalies between the sub-polar gyre and the Northern
216 Hemisphere while the $\delta^{18}O$ captures the temperature and water mass distribution of the slope
217 water. Despite the potential caveats, the similarity between our $\delta^{18}O$ record, the temperature-
218 based AMOC index, and instrumental data adds to the evidence linking the strength of the
219 AMOC with the western North Atlantic subsurface temperature (Marcott et al., 2011; Petrie &
220 Drinkwater, 1993; Saba et al., 2016), which implies that temperature can been used to diagnose
221 the state of AMOC, as done previously (Caesar et al., 2018; Rahmstorf et al., 2015; Thornalley
222 et al., 2018; Zhang, 2008). The $\delta^{18}O$ of benthic foraminifera in the Laurentian Channel can
223 thus provide crucial information to reconstruct AMOC variability during the last century
224 despite the fact that it incorporates both the temperature and the water mass signal.

225   The trend of $\delta^{18}O$ derived from the benthic foraminifera in long piston core MD99-
226 2220 (hereafter MD) during the 20th century is unique in its magnitude for the last 1,500 years.
227 While the current global warming trend could be invoked to explain this warming, we stress
228 that neither of the parent water masses warmed significantly during the same period (Gilbert
229 et al., 2005). Moreover, the absolute value of 1.5-2.0°C is much larger than the ~0.4°C
230 attributed to the global trend (IPCC, 2013). Potential control from the North Atlantic
231 Oscillation can also be discarded as no correlation with the temperature time series was
232 observed (Gilbert et al., 2005). While still controversial, the reduction of the AMOC since the
233 late 1930s and the drastic shift in North Atlantic overturning cell at the beginning of the 70's

234 was already identified using field data (Dima & Lohmann, 2010). The agreement between the
235 instrumental data, various climate archives, the two models, and the AMOC index lead us to
236 conclude that the weakening of the AMOC is a major factor causing the sub-surface warming
237 recorded in the sediment cores and corals compiled here. The evidence presented here thus
238 reinforces previous findings and provides complementary proxy-based evidence for the 20th
239 century AMOC slowdown.

240   While our record and modeling results strengthens the previous hypothesis regarding the
241 recent weakening of the AMOC and its consequences in the western North Atlantic, it also
242 highlights some discrepancies such as the 100-year difference in the beginning of the
243 weakening of the convection in the Labrador Sea (Thornalley et al., 2018) and the AMOC
244 (Caesar et al., 2018; Rahmstorf et al., 2015). Interestingly, our $\delta^{18}O$ record, interpreted as
245 being controlled by DWBC strength, mimics the AMOC index with a weakening starting
246 within the last century as opposed to the 19th century decline in the Labrador Sea convection
247 (Thornalley et al., 2018). While it is conceivable to invoke a potential lag between a reduced
248 convection in the Labrador Sea and its expression on surface waters, the pre-AD 1200
249 paleorecord does not seem to exhibit such lag, as the $\delta^{18}O$ matches the proxy for convection in
250 the Labrador Sea (Fig 4; see section 3.5). However, the amplitude of the recent weakening is
251 unique over this period and so caution should be exercised when directly using the paleorecord
252 to find the cause of this apparent mismatch. Moreover, the potential absence of decline in
253 Labrador Sea convection during the last part of 20th century (Böning et al., 2016) and the last
254 couple of decades (Yashayaev & Loder, 2016) also highlight the need to reconcile estimation
255 of convection in the Labrador Sea and the integrative AMOC proxies.

256   While it is possible to use our $\delta^{18}O$ proxy in longer reconstruction, it is not possible to
257 constrain $\delta^{18}O$ change solely to a change in the proportion of water masses as we did for the
258 last century since it is not known if the parent water masses temperature varied. As such,
259 potential temperature changes of the Gulf Stream (and ATSW) and Labrador Current (and
260 LSSW) should also be considered as a potential driver of $\delta^{18}O$ when analysing the pre-20th
261 century record.

262

263 *3.4. The 1600-1900 period*

264   While we observe a step-wise decrease in the AMOC starting in the late 15th century,
265 these variations are within the natural range of variability of our $\delta^{18}O$ record (Fig S6). However,

266   the 1600-1899 δ^{18}O values in core MD are significantly heavier compared to the pre-1600

267   record, suggesting a statistically weaker AMOC during the LIA. Alternative explanations for

268   the low δ^{18}O during this period include a warming of either parent water mass, which would

269   be counterintuitive for this time period (Keigwin, 1996). While the δ^{18}O of the Gulf Stream

270   increased by about 0.1 ‰ between 1600 and 1900 (Saenger et al., 2011), it would account only

271   for half of the increase observed in the MD core. Thus, a change in the proportion of the water

272   masses entering the Laurentian Channel due to a weaker AMOC cannot be excluded at this

273   point. At about AD 1850-1875, the sharp depletion in δ^{18}O is synchronous with the sudden

274   decrease in DWBC intensity and Labrador Sea convection, which might be due to the

275   beginning of the post-LIA ice cap melt and the consequent freshening of the Labrador Sea

276   surface water (Koerner, 1977; Koerner & Fisher, 1990). While the MD core might record a

277   weakened AMOC state during most of the LIA (1625-1850), its step-wise nature, rather than a

278   continual weakening trend observed in the sortable silt record highlights a potential

279   discrepancy between how the AMOC intensity is expressed in the δ^{18}O record and how it is

280   translated in current velocity at 2,000 m depth, where the 48JPC and 56JPC cores were

281   retrieved (Thornalley et al., 2018). Here, the potential interference from temperature and

282   salinity changes in the parent water masses should be investigated in greater detail.

283

284   *3.5. The pre-1600 period*

285   The comparison of the MD core with the AMOC index highlights the absence of any

286   trend within these two records throughout this period (Fig 4a). However, the MD record is

287   characterized by more variability pre-AD 1500. This may be caused by the construction of the

288   AMOC index based on multiple different proxies of SST in both the western North Atlantic

289   and the subpolar North Atlantic, whereas the MD core records the subsurface signal at a single

290   location, implying that the AMOC index integrates a much larger oceanic area and reduces the

291   variability (Rahmstorf et al., 2015). This might alternatively be explained by subsurface

292   temperature being slightly more sensitive to convection relative to the surface temperature.

293   This is supported by the agreement pre-AD 1500 between the MD core and temperature and

294   salinity reconstructions from the Labrador Sea (Fig 4b), which are considered effective proxies

295   for Labrador Sea convection (Moffa-Sánchez et al., 2014). Thus, the δ^{18}O seems to record most

296   of the natural variability of the Labrador Sea convection over that period.

297

298 **4. Implications**

299 Our record adds to the very few existing paleoreconstructions of AMOC for the last millennium

300 and highlights the statistically weaker state of the AMOC during the 20th century. While our

301 record substantiates previous finding, it also provides a unique high-resolution record of

302 western North Atlantic sub-surface water evolution for the last millennium. The data provided

303 here are thus important to disentangle the potential causes of the 20th century weakening, as

304 they record sub-surface processes, which is different from the previously-published surface

305 AMOC index (Caesar et al., 2018; Rahmstorf et al., 2015) and reconstruction of the DWBC

306 (Thornalley et al., 2018). Moreover, the heavy $\delta^{18}O$ recorded during the LIA suggests a

307 potential weakening of the AMOC during that period. These data could be used with

308 temperature reconstructions of the Labrador current and Gulf Stream in order to further

309 constrain the implication of the heavy $\delta^{18}O$ values during the LIA. By discussing the

310 similarities and discrepancies between the records during the 20th century and LIA we provided

311 new insights on the role of the Labrador Current in both weakening event but also the need to

312 reconcile the different AMOC record with modern instrumental data. Our $\delta^{18}O$ record thus

313 captures crucial information that will contribute to a better understanding of AMOC variability

314 throughout the last 1,500 years and its drivers.

315

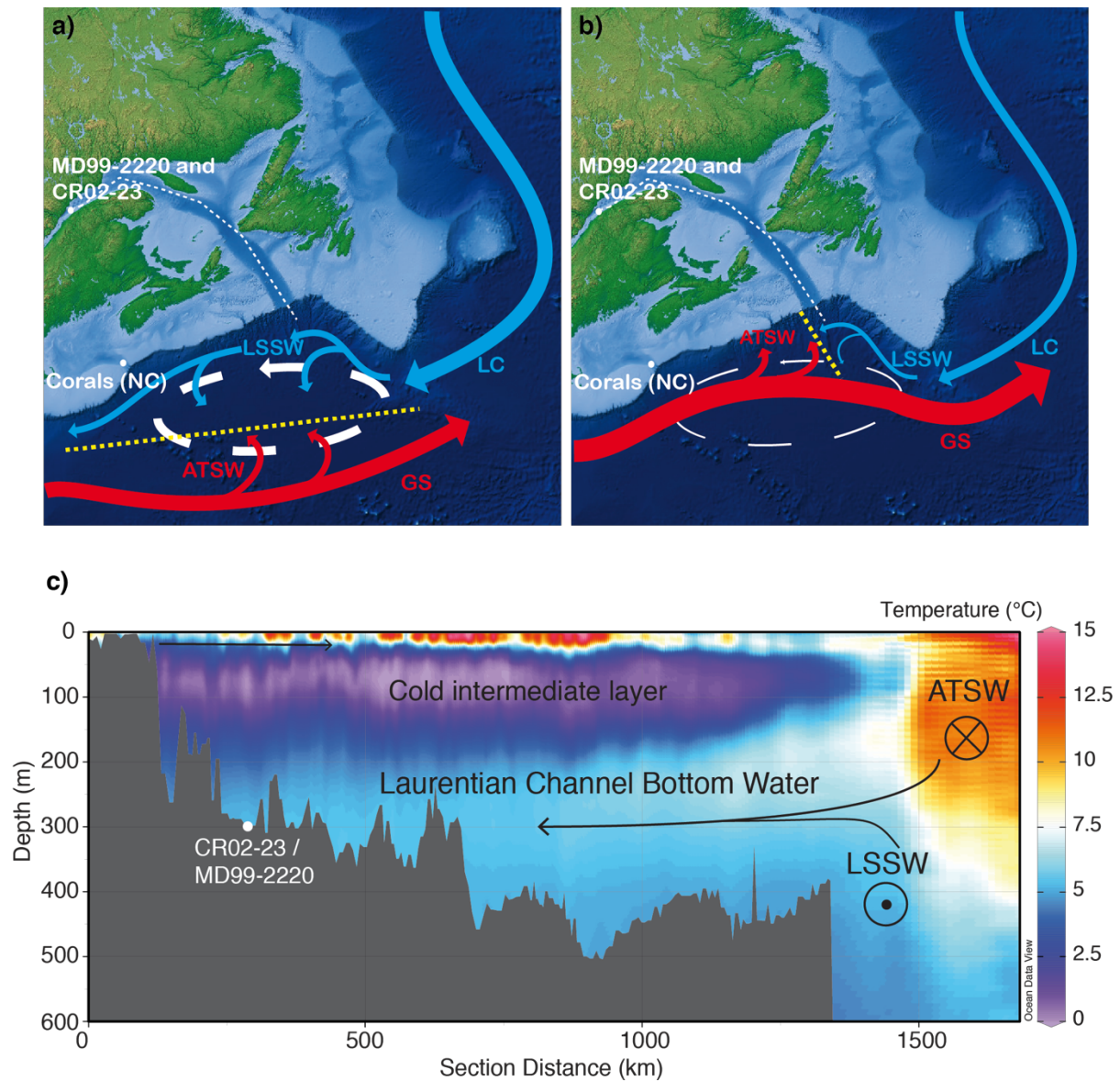328   **Figures and Tables**
329

330

331

332   **Figure 1. Link between the strength of convection in the Labrador Sea, the**
333   **westward transport of Labrador current and the temperature across the Laurentian**
334   **Channel.** Schematic diagram of oceanic circulation near the entrance of the Laurentian
335   Channel in episodes of **a)** strong westward transport of Labrador Current (LC) and Labrador
336   Sea Slope Water (LSSW) with weaker influence of Atlantic Temperate Slope Water (ATSW)
337   derived from the Gulf Stream (GS) and **b)** weak westward transport of Labrador current and **c)**
338   the 2000-2010 averaged temperature (Levitus et al., 2013) profile along the Laurentian
339   Channel. The oceanography of the Northwest Atlantic is characterized by the interaction
340   between water masses formed in the Labrador Sea moving southward and the northward

341 flowing Gulf Stream. The exact location where these two water mass systems meet (yellow

342 dashed lines) is determined by the strength of the northern recirculation gyre (white arrows)

343 (Hogg et al., 1986). The width of the arrows represents the relative strength of the current.

344 White dots indicate the position of core MD99-2220 and CR02-23, which were cored close to

345 each other (respectively at; 48°38.32'N, 68°37.93'W; 320m and 48°42.01'N, 68°38.89'W;

346 345m). The position of corals raised from the Northeast Channel where a δ^{15}N time series was

347 recorded is also marked (42°00'N, 65°36'W, between 275 and 450 m) (Sherwood et al., 2011).

348 The temperature profile depicts the annually averaged position of the slope waters and how

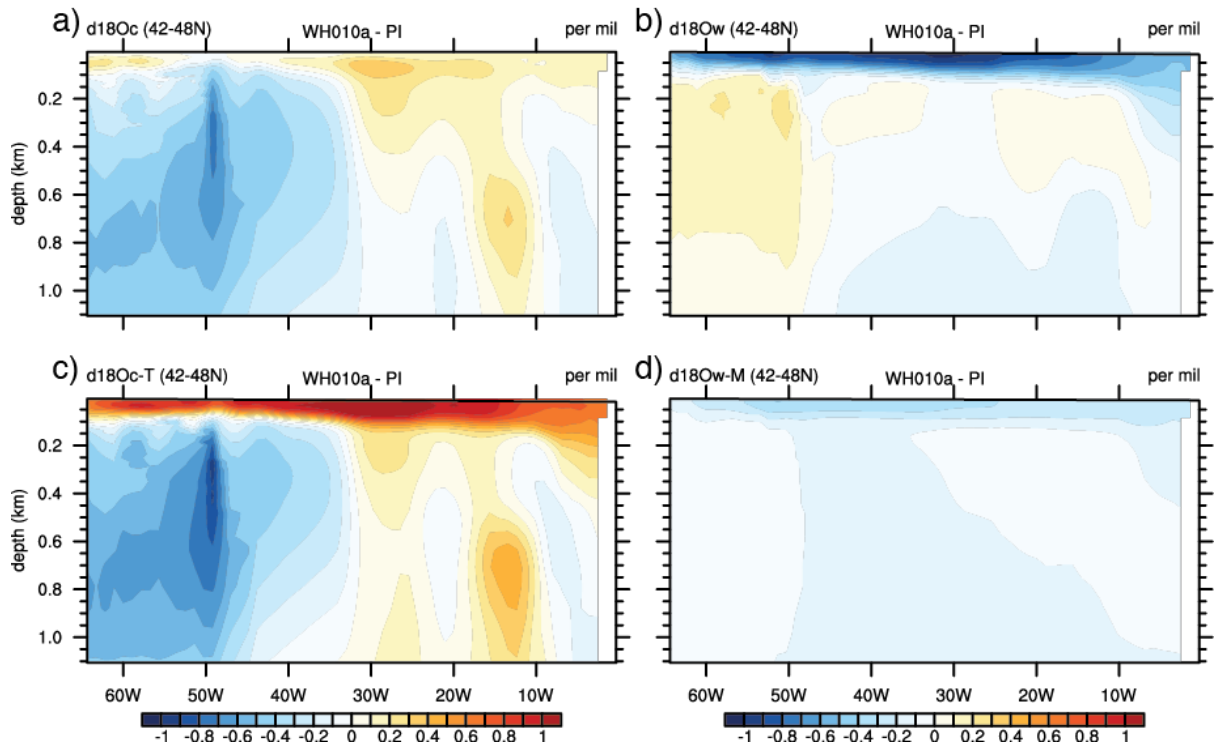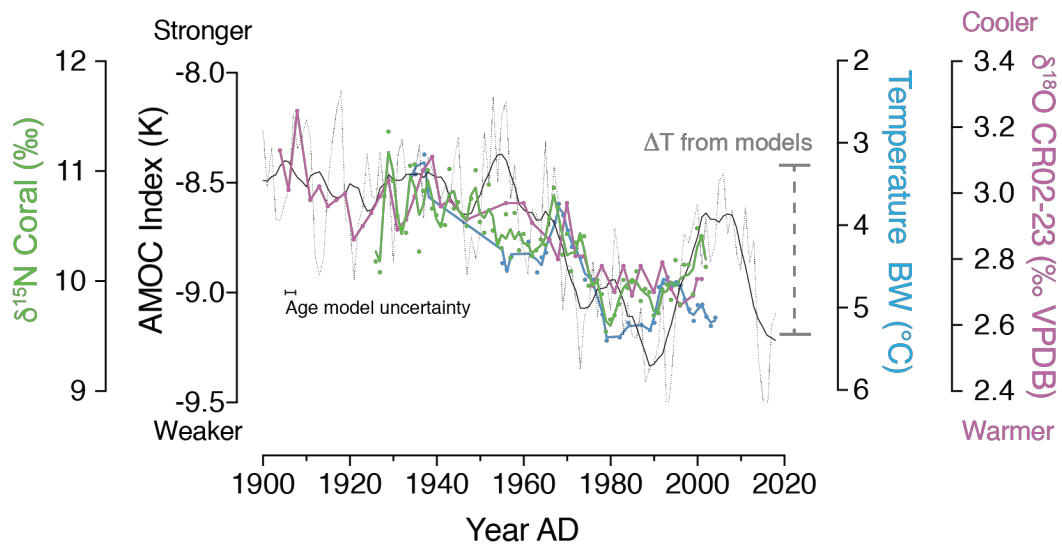349 they fill the bottom of the Laurentian Channel.

350

Figure 2. Attributing response of subsurface carbonate $\delta^{18}O$ to freshwater forcing in iCESM. a) Total changes in carbonate $\delta^{18}O$ (units: ‰ PDB) along 45°N in the North Atlantic calculated from modeled changes in seawater $\delta^{18}O$ (units: ‰ SMOW) and ocean temperature using the equation of Shackleton (1974), and contributions from **b)** changes in seawater $\delta^{18}O$ and **c)** ocean temperature. **d)** changes in seawater $\delta^{18}O$ (units: ‰ SMOW) coming from the direct meltwater effect, that is the direct depletion from the depleted freshwater forcing without changes in circulations.
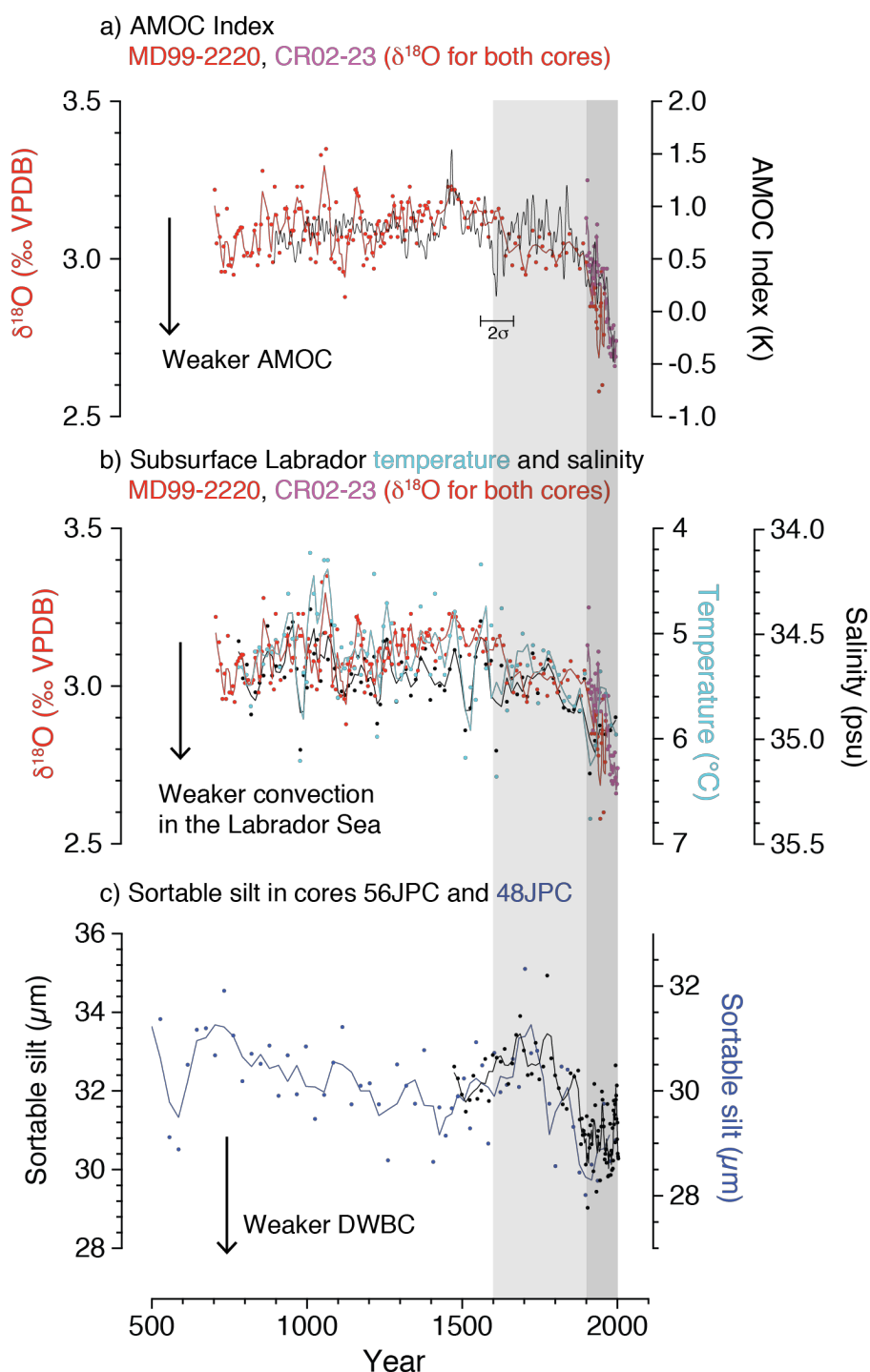
361

362

363   **Figure 3. Proxy validation using instrumental data and paleorecords.** The AMOC

364   index (Caesar et al., 2018) (black dotted line and smoothed black dashed line; 2nd order; 8

365   neighbors) and instrumental temperature record of Laurentian Channel bottom water (Gilbert

366   et al., 2005) (light blue dots and smoothed line; 2nd order, 2 neighbors) are plotted for the 1900-

367   2000 period along the annually resolved coral δ^{15}N record (Sherwood et al., 2011) (green dots

368   and smoothed line; 2nd order, 2 neighbors) that serves as a proxy of the strength of the northern

369   recirculation gyre and the modal state of the western North Atlantic circulation. The δ^{18}O of

370   benthic foraminifera from core CR02-23 (Thibodeau et al., 2010a) (pink) also shows the same

371   general pattern during that period. The average temperature increase (2°C) obtained at 400 m

372   deep in the western North Atlantic in our modelled AMOC-weakening experiments is indicated

373   by the gray bracket. An offset of 1.8 years was found between the lead-based age model and

374   the cesium peak and used to quantify the uncertainty, this offset is shown on the figure. The

375   analytical uncertainty of the lead-base age model (2σ) was found to be much smaller than the

376   offset displayed on the figure (S1).

377

378

a) AMOC Index
MD99-2220, CR02-23 (δ¹⁸O for both cores)

b) Subsurface Labrador temperature and salinity
MD99-2220, CR02-23 (δ¹⁸O for both cores)

c) Sortable silt in cores 56JPC and 48JPC

379

Figure 4. Comparison of North Atlantic climate archives covering the last millennium. The first panel **a)** comparison of composite (MD99-2220; red and CR02-23; pink) δ¹⁸O *Globobulimina auriculata* record (smoothed lines; 2ⁿᵈ order, 2 neighbors) with the AMOC index (Rahmstorf et al., 2015) (black line). **b)** similarity of the composite (MD99-2220; red and CR02-23; pink) δ¹⁸O record (smoothed lines; 2ⁿᵈ order, 2 neighbors) with reconstructed subsurface temperature (light blue dots) and salinity (black dots) of the Labrador Sea (Moffa-

386   Sánchez et al., 2014), which are indicative of convection in the Labrador Sea (smoothed lines;

387   2nd order, 2 neighbors). **c)** sortable silt from two sediment cores retrieved off Cape Hatteras, a

388   proxy of the deep western boundary current (smoothed lines; 2nd order, 2 neighbors)

389   (Thornalley et al., 2018). Grey bars highlight the LIA and the 20th century. The 2σ value linked

390   to ^{14}C dating of core MD99-2220 (St-Onge et al., 2003) is shown on the graph.

391

392

393 Bakker, P., Schmittner, A., Lenaerts, J. T. M., Abe-Ouchi, A., Bi, D., van den Broeke, M. R.,
394   et al. (2016). Fate of the Atlantic Meridional Overturning Circulation: Strong decline
395   under continued warming and Greenland melting. *Geophysical Research Letters*,
396   *43*(23), 12,252-12,260. https://doi.org/10.1002/2016GL070457

397 Benoit, P., Gratton, Y., & Mucci, A. (2006). Modeling of dissolved oxygen levels in the
398   bottom waters of the Lower St. Lawrence Estuary: Coupling of benthic and pelagic
399   processes. *Marine Chemistry*, *102*(1–2), 13–32.
400   https://doi.org/10.1016/j.marchem.2005.09.015

401 Bohm, E., Lippold, J., Gutjahr, M., Frank, M., Blaser, P., Antz, B., et al. (2015). Strong and
402   deep Atlantic meridional overturning circulation during the last glacial cycle. *Nature*,
403   *517*(7532), 73–76. Retrieved from http://dx.doi.org/10.1038/nature14059

404 Böning, C. W., Behrens, E., Biastoch, A., Getzlaff, K., & Bamber, J. L. (2016). Emerging
405   impact of Greenland meltwater on deepwater formation in the North Atlantic Ocean.
406   *Nature Geosci*, *9*(7), 523–527. Retrieved from http://dx.doi.org/10.1038/ngeo2740

407 Brickman, D., Hebert, D., & Wang, Z. (2018). Mechanism for the recent ocean warming
408   events on the Scotian Shelf of eastern Canada. *Continental Shelf Research*, *156*, 11–22.
409   https://doi.org/10.1016/j.csr.2018.01.001

410 Caesar, L., Rahmstorf, S., Robinson, A., Feulner, G., & Saba, V. (2018). Observed
411   fingerprint of a weakening Atlantic Ocean overturning circulation. *Nature*, *556*(7700),
412   191–196. https://doi.org/10.1038/s41586-018-0006-5

413 Curry, R. (2005). Dilution of the Northern North Atlantic Ocean in Recent Decades. *Science*,
414   *308*(5729), 1772–1774. https://doi.org/10.1126/science.1109477

415 Delworth, T. L., Clark, P. U., Holland, M., Johns, W. E., Kuhlbrodt, T., Lynch-Stieglitz, J., et
416   al. (2008). The Potential for Abrupt Change in the Atlantic Meridional Overturning
417   Circulation. *Abrupt Climate Change*, 117–162. Retrieved from
418   http://citeseerx.ist.psu.edu/viewdoc/download?doi=10.1.1.184.709&rep=rep1&type=pdf
419   %5Cnhttp://downloads.climatescience.gov/sap/sap3-4/sap3-4-final-report-ch4.pdf

420 Dima, M., & Lohmann, G. (2010). Evidence for Two Distinct Modes of Large-Scale Ocean
421   Circulation Changes over the Last Century. *Journal of Climate*, *23*(1), 5–16.
422   https://doi.org/10.1175/2009JCLI2867.1

423 Gilbert, D., Sundby, B., Gobeil, C., Mucci, A., & Tremblay, G. H. (2005). A seventy-two-
424   year record of diminishing deep-water oxygen in the St. Lawrence estuary: The
425   northwest Atlantic connection. *Limnology and Oceanography*, *50*(5), 1654–1666.
426   https://doi.org/10.4319/lo.2005.50.5.1654

427 Gregory, J. M., Dixon, K. W., Stouffer, R. J., Weaver, A. J., Driesschaert, E., Eby, M., et al.
428   (2005). A model intercomparison of changes in the Atlantic thermohaline circulation in
429   response to increasing atmospheric CO2 concentration. *Geophysical Research Letters*,
430   *32*(12), 1–5. https://doi.org/10.1029/2005GL023209

431 Hillaire-Marcel, C., & Causse, C. (1989). The late pleistocene Laurentide glacier: Th U
432   dating of its major fluctuations and δ18O range of the ice. *Quaternary Research*, *32*(2),
433   125–138. https://doi.org/10.1016/0033-5894(89)90070-7

434 Hogg, N. G., Pickart, R. S., Hendry, R. M., & Smethie, W. J. (1986). The northern
435   recirculation gyre of the gulf Stream. *Deep Sea Research Part A, Oceanographic
436   Research Papers*, *33*(9), 1139–1165. https://doi.org/10.1016/0198-0149(86)90017-8

437 IPCC. (2013). *Climate Change 2013: The Physical Science Basis. Summary for
438   Policymakers*. *IPCC*. Retrieved from
439   http://medcontent.metapress.com/index/A65RM03P4874243N.pdf

440 Jungclaus, J. H., Haak, H., Esch, M., Roeckner, E., & Marotzke, J. (2006). Will Greenland
441   melting halt the thermohaline circulation? *Geophysical Research Letters*, *33*(17).
442   https://doi.org/10.1029/2006GL026815

443 Keigwin, L. D. (1996). The Little Ice Age and Medieval Warm Period in the Sargasso Sea.
444   *Science*, *274*(5292), 1503–1508. https://doi.org/10.1126/science.274.5292.1503
445 Koerner, R. M. (1977). Devon Island Ice Cap: Core Stratigraphy and Paleoclimate. *Science*,
446   *196*(4285), 15–18. https://doi.org/10.1126/science.196.4285.15
447 Koerner, R. M., & Fisher, D. A. (1990). A record of Holocene summer climate from a
448   Canadian high-Arctic ice core. *Nature*, *343*(6259), 630–631.
449   https://doi.org/10.1038/343630a0
450 Krebs, U., & Timmermann, A. (2007). Fast advective recovery of the Atlantic meridional
451   overturning circulation after a Heinrich event. *Paleoceanography*, *22*(1), 1–9.
452   https://doi.org/10.1029/2005PA001259
453 Lefort, S., Gratton, Y., Mucci, a., Dadou, I., & Gilbert, D. (2012). Hypoxia in the Lower St.
454   Lawrence Estuary: How physics controls spatial patterns. *Journal of Geophysical*
455   *Research*, *117*(C7), C07018. https://doi.org/10.1029/2011JC007751
456 LeGrande, A. N., & Schmidt, G. A. (2006). Global gridded data set of the oxygen isotopic
457   composition in seawater. *Geophysical Research Letters*, *33*(12).
458   https://doi.org/10.1029/2006GL026011
459 Levitus, S., Antonov, J. I., Baranova, O. K., Boyer, T. P., Coleman, C. L., Garcia, H. E., et al.
460   (2013). The World Ocean Database. *Data Science Journal*, *12*(0), WDS229-WDS234.
461   https://doi.org/10.2481/dsj.WDS-041
462 Liu, W., Xie, S.-P., Liu, Z., & Zhu, J. (2017). Overlooked possibility of a collapsed Atlantic
463   Meridional Overturning Circulation in warming climate. *Science Advances*, *3*(1).
464   Retrieved from http://advances.sciencemag.org/content/3/1/e1601666.abstract
465 Luo, H., Castelao, R. M., Rennermalm, A. K., Tedesco, M., Bracco, A., Yager, P. L., &
466   Mote, T. L. (2016). Oceanic transport of surface meltwater from the southern Greenland
467   ice sheet. *Nature Geoscience*, *9*(7), 528–532. https://doi.org/10.1038/ngeo2708
468 Marcott, S. A., Clark, P. U., Padman, L., Klinkhammer, G. P., Springer, S. R., Liu, Z., et al.
469   (2011). Ice-shelf collapse from subsurface warming as a trigger for Heinrich events.
470   *Proceedings of the National Academy of Sciences of the United States of America*,
471   *108*(33), 13415–13419. https://doi.org/10.1073/pnas.1104772108
472 Moffa-Sánchez, P., Hall, I. R., Barker, S., Thornalley, D. J. R., & Yashayaev, I. (2014).
473   Surface changes in the eastern Labrador Sea around the onset of the Little Ice Age.
474   *Paleoceanography*, *29*(3), 160–175. https://doi.org/10.1002/2013PA002523
475 Nusbaumer, J., Wong, T. E., Bardeen, C., & Noone, D. (2017). Evaluating hydrological
476   processes in the Community Atmosphere Model Version 5 (CAM5) using stable isotope
477   ratios of water. *Journal of Advances in Modeling Earth Systems*, *9*(2), 949–977.
478   https://doi.org/10.1002/2016MS000839
479 Petrie, B., & Drinkwater, K. (1993). Temperature and salinity variability on the Scotian Shelf
480   and in the Gulf of Maine 1945–1990. *Journal of Geophysical Research*, *98*(C11),
481   20079. https://doi.org/10.1029/93JC02191
482 Rahmstorf, S., Box, J. E., Feulner, G., Mann, M. E., Robinson, A., Rutherford, S., &
483   Schaffernicht, E. J. (2015). Exceptional twentieth-century slowdown in Atlantic Ocean
484   overturning circulation. *Nature Climate Change*, *5*(5), 475–480.
485   https://doi.org/10.1038/nclimate2554
486 Ravelo, A. C., & Hillaire-Marcel, C. (2007). The Use of Oxygen and Carbon Isotopes of
487   Foraminifera in Paleoceanography. In *Developments in Marine Geology* (Vol. 1, pp.
488   735–764). https://doi.org/10.1016/S1572-5480(07)01023-8
489 Saba, V. S., Griffies, S. M., Anderson, W. G., Winton, M., Alexander, M. A., Delworth, T.
490   L., et al. (2016). Enhanced warming of the Northwest Atlantic Ocean under climate
491   change. *Journal of Geophysical Research: Oceans*, *121*(1), 118–132.
492   https://doi.org/10.1002/2015JC011346

493 Saenger, C., Came, R. E., Oppo, D. W., Keigwin, L. D., & Cohen, A. L. (2011). Regional
494   climate variability in the western subtropical North Atlantic during the past two
495   millennia. *Paleoceanography*, *26*(2). https://doi.org/10.1029/2010PA002038
496 Schmittner, A., & Lund, D. C. (2015). Early deglacial Atlantic overturning decline and its
497   role in atmospheric CO2 rise inferred from carbon isotopes (d13C). *Climate of the Past*,
498   *11*(2), 135–152. https://doi.org/10.5194/cp-11-135-2015
499 Shackleton, N. J. (1974). Attainment of isotopic equilibrium between ocean water and the
500   benthonic foraminifera geuns *Uvigerina*: Isotopic changes in the ocean during the last
501   glacial. *Colloques Internationaux Du C.N.R.S.*, *219*, 203–210.
502 Sherwood, O. A., Lehmann, M. F., Schubert, C. J., Scott, D. B., & McCarthy, M. D. (2011).
503   Nutrient regime shift in the western North Atlantic indicated by compound-specific
504   δ15N of deep-sea gorgonian corals. *Proceedings of the National Academy of Sciences of
505   the United States of America*, *108*(3), 1011–5. https://doi.org/10.1073/pnas.1004904108
506 St-Onge, G., Stoner, J. S., & Hillaire-Marcel, C. (2003). Holocene paleomagnetic records
507   from the St. Lawrence Estuary, eastern Canada: centennial- to millennial-scale
508   geomagnetic modulation of cosmogenic isotopes. *Earth and Planetary Science Letters*,
509   *209*(1–2), 113–130. https://doi.org/10.1016/S0012-821X(03)00079-7
510 Stouffer, R. J., Yin, J., Gregory, J. M., Dixon, K. W., Spelman, M. J., Hurlin, W., et al.
511   (2006). Investigating the Causes of the Response of the Thermohaline Circulation to
512   Past and Future Climate Changes. *Journal of Climate*, *19*(8), 1365–1387.
513   https://doi.org/10.1175/JCLI3689.1
514 Thibodeau, B., de Vernal, A., & Mucci, A. (2006). Recent eutrophication and consequent
515   hypoxia in the bottom waters of the Lower St. Lawrence Estuary: Micropaleontological
516   and geochemical evidence. *Marine Geology*, *231*(1–4), 37–50.
517   https://doi.org/10.1016/j.margeo.2006.05.010
518 Thibodeau, B., Lehmann, M. F., Kowarzyk, J., Mucci, A., Gélinas, Y., Gilbert, D., et al.
519   (2010). Benthic nutrient fluxes along the Laurentian Channel: Impacts on the N budget
520   of the St. Lawrence marine system. *Estuarine, Coastal and Shelf Science*, *90*(4), 195–
521   205. https://doi.org/10.1016/j.ecss.2010.08.015
522 Thibodeau, B., de Vernal, A., Hillaire-Marcel, C., & Mucci, A. (2010). Twentieth century
523   warming in deep waters of the Gulf of St. Lawrence: A unique feature of the last
524   millennium. *Geophysical Research Letters*, *37*(17).
525   https://doi.org/10.1029/2010GL044771
526 Thibodeau, B., de Vernal, A., & Limoges, A. (2013). Low oxygen events in the Laurentian
527   Channel during the Holocene. *Marine Geology*, *346*, 183–191.
528   https://doi.org/10.1016/j.margeo.2013.08.004
529 Thornalley, D. J. R., Oppo, D. W., Ortega, P., Robson, J. I., Brierley, C. M., Davis, R., et al.
530   (2018). Anomalously weak Labrador Sea convection and Atlantic overturning during the
531   past 150 years. *Nature*, *556*(7700), 227–230. https://doi.org/10.1038/s41586-018-0007-4
532 Wong, T. E., Nusbaumer, J., & Noone, D. C. (2017). Evaluation of modeled land-atmosphere
533   exchanges with a comprehensive water isotope fractionation scheme in version 4 of the
534   Community Land Model. *Journal of Advances in Modeling Earth Systems*, *9*(2), 978–
535   1001. https://doi.org/10.1002/2016MS000842
536 Yang, Q., Dixon, T. H., Myers, P. G., Bonin, J., Chambers, D., & Van Den Broeke, M. R.
537   (2016). Recent increases in Arctic freshwater flux affects Labrador Sea convection and
538   Atlantic overturning circulation. *Nature Communications*, *7*.
539   https://doi.org/10.1038/ncomms10525
540 Yashayaev, I., & Loder, J. W. (2016). Recurrent replenishment of Labrador Sea Water and
541   associtated decadal-scale variability. *Journal Geophysical Research: Oceans*, *121*,
542   8095–8114. https://doi.org/10.1002/2016JC012046.Received

543   Yu, L., Gao, Y., & Otterå, O. H. (2016). The sensitivity of the Atlantic meridional
544   overturning circulation to enhanced freshwater discharge along the entire, eastern and
545   western coast of Greenland. *Climate Dynamics*, *46*(5–6), 1351–1369.
546   https://doi.org/10.1007/s00382-015-2651-9
547   Zhang, J., Liu, Z., Brady, E. C., Oppo, D. W., Clark, P. U., Jahn, A., et al. (2017).
548   Asynchronous warming and δ 18 O evolution of deep Atlantic water masses during the
549   last deglaciation. *Proceedings of the National Academy of Sciences*, *114*(42), 11075–
550   11080. https://doi.org/10.1073/pnas.1704512114
551   Zhang, R. (2008). Coherent surface-subsurface fingerprint of the Atlantic meridional
552   overturning circulation. *Geophysical Research Letters*, *35*(20), L20705.
553   https://doi.org/10.1029/2008GL035463
554   Zhang, R., Vallis, G. K., Fluid, G., Oceanic, N., & Program, O. S. (2007). The Role of
555   Bottom Vortex Stretching on the Path of the North Atlantic Western Boundary Current
556   and on the Northern Recirculation Gyre. *Journal of Physical Oceanography*, *37*(8),
557   2053–2080. https://doi.org/10.1175/JPO3102.1
558   Zhu, J., Liu, Z., Brady, E. C., Otto-Bliesner, B. L., Marcott, S. A., Zhang, J., et al. (2017).
559   Investigating the Direct Meltwater Effect in Terrestrial Oxygen-Isotope Paleoclimate
560   Records Using an Isotope-Enabled Earth System Model. *Geophysical Research Letters*,
561   *44*, 12501–12510. https://doi.org/10.1002/2017GL076253
562   Zhu, J., Liu, Z., Brady, E., Otto-Bliesner, B., Zhang, J., Noone, D., et al. (2017). Reduced
563   ENSO variability at the LGM revealed by an isotope-enabled Earth system model.
564   *Geophysical Research Letters*, *44*(13), 6984–6992.
565   https://doi.org/10.1002/2017GL073406
566
567

568   **Supporting information for:**

569   Last century warming over the Canadian Atlantic shelves linked to weak
570   Atlantic Meridional Overturning Circulation

571

572

573   **Authors**

574   B. Thibodeau[1,2]†[*], C. Not[1,2]†, J. Zhu[3], A. Schmittner[4], D. Noone[4], C. Tabor[5], J. Zhang[6], Z.
575   Liu[7]

576

577   **Affiliations**
578   [1]Department of Earth Sciences, The University of Hong Kong, Hong Kong SAR

579   [2]The Swire Institute of Marine Science, The University of Hong Kong, Hong Kong SAR

580   [3]Department of Earth and Environmental Sciences, University of Michigan, United-States of
581   America

582   [4]College of Earth, Ocean, and Atmospheric Sciences, Oregon State University, United-States
583   of America

584   [5]Center for Integrative Geosciences, University of Connecticut, United-States of America

585   [6]CCS-2 and CNLS, Los Alamos National Laboratory, Los Alamos, New Mexico, United-
586   States of America

587   [7]Atmospheric Science Program, Department of Geography, The Ohio State University,
588   United-States of America

589

590   *Correspondence to: bthib@hku.hk

591   † Equal contribution

592

593

594

595   **Content**

596   Text S1 to S5

597   Figures S1 to S5

598

599   **Additional file**

600   Full dataset (excel file)

601

602   **Introduction**

603   This file includes additional details about modeling results, sediment cores chronology and

604   uncertainty of the proxy used as well as statistic on the results.

605

606   **1. Chronostratigraphy of climate archives**

607   The chronostratigraphy of core MD99-2220 was originally established by St-Onges et

608   al. (2003) based on twenty benthic mollusk shells analyzed from MD99-2220 and neighbor

609   core MD99-2221. Correlation with a box core retrieved from the same site indicated that the

610   top 14 cm of core MD99-2220 was missing. The age model of the upper part of core MD99-

611   2220 was established using a box-core retrieved from the same vicinity. The cross-correlation

612   between MD99-2220 and AH00-2220 was performed based on geochemical data (St-Onge et

613   al., 2003; Thibodeau et al., 2006; Thibodeau et al., 2010a). The chronostratigraphy of box core

614   CR02-23 (taken at the same site) was validated using ^{210}Pb (Thibodeau et al., 2006). Here we

615   present an updated age model for both cores using a constant-rate supply ^{210}Pb model that

616   calculates variable sedimentation rate for each sample, which is particularly suitable for last-

617   century cores where sedimentation rate often changes due to anthropogenic activities (Ghaleb,

618   2009) (Fig S4). We calculated the analytical uncertainty using the constant initial concentration

619   model, which respectively yielded error of $\pm$ 0.16 and 0.14 year per cm ($\pm$ 2σ) for core AH00-

620   2220 and CR02-23. An offset of 1.8 years was found between the lead-based age model and

621   the cesium-137 peak. (Fig S3). Due to the loss of the top 14 cm of core MD99-2220, we will

622   not use this core for high-resolution reconstruction of the last century and rather focus on core

623   CR02-23. While the benthic foraminifera δ^{18}O values are similar for both cores and decrease

624   toward the younger part of the core, there is an offset of about 40 years between the appearance

625   of the lowest value in the two cores (Fig S4). This offset could be due to sediment

626   disturbance/compression in the upper part of the piston core.

627   The chronostratigraphy of gorgonian coral was done using band-counting validated by

628   radiocarbon measurement (Sherwood et al., 2011). The subsurface Labrador Sea temperature

629   and salinity record comes from sediment core RAPiD-35-25B (Moffa-Sánchez et al., 2014).

630   We used the original chronology, which is based on ^{210}Pb dating of the upper part of the core

631   and seven ^{14}C dates in the older part of the core (Moffa-Sánchez et al., 2014).

632

633   **2. Uncertainties of different proxies**

634   Measurement of δ^{18}O in core MD99-2220 and CR02-23 was performed with an

635   analytical precision better than $\pm$0.05 ‰, which is equivalent to a precision of about 0.15-

636   0.20°C in temperature. Instrumental measurements of Laurentian Channel bottom water

637   temperature were carried out with a precision of $\pm$0.01°C (Gilbert et al., 2005). Nitrogen

638   isotopes of coral were measured with an analytical precision better than ±0.20‰ (Sherwood et
639   al., 2011). Subsurface salinity and temperature reconstruction of the Labrador Sea have an
640   uncertainty of ±0.8 psu and ±0.8°C (Moffa-Sánchez et al., 2014). Analytical precision for
641   sortable silt was estimated at 1% (±0.3 μm), while replicates-based precision was estimated at
642   ±0.8 μm (Thornalley et al., 2018).

643

644   **3. Modeling results**

645   In response to the freshwater forcing (0.05 Sv in the UVic and 0.10 Sv in the iCESM),
646   the upper-ocean seawater becomes fresher and lighter, increasing stratification and inhibiting
647   deep convection in the North Atlantic (Fig S1). As a result, the AMOC strength, indicated by
648   the maximum transport in the North Atlantic, decreases by 17% and 28% in 100 years in UVic
649   and iCESM, respectively. The warming is a consequence of reduced northward transport in the
650   Gulf Stream, which requires a decrease in zonal density (temperature) gradients via thermal
651   wind balance. The models achieve this by warming west and cooling east of ~40°W. Modeling
652   results suggest that the reorganization of gyre circulations is a direct consequence of AMOC
653   weakening (Saba et al., 2016; Thornalley et al., 2018). The reduced northward heat transport
654   associated with the AMOC decreases the SST in the northern North Atlantic significantly and
655   produces a local high-pressure anomaly (Stouffer et al., 2006). The high-pressure anomaly acts
656   to weaken the westerlies in the mid-latitude North Atlantic and the gyre circulations. A budget
657   analysis of the subsurface temperature changes in iCESM was conducted. The analysis
658   suggests that the net subsurface warming is primarily caused by the reduced zonal component
659   of the Gulf Stream, as the reduced meridional flow acts to cool the subsurface water (Fig S2).
660   It is important to note that we only applied freshwater forcing at the ocean surface and kept all
661   other boundary conditions and forcings constant, as the parent water masses did not warm
662   during the last century (Gilbert et al., 2005). Therefore, the subsurface temperature increase is
663   solely due to a change in the circulation. In summary, both models suggest a warming of
664   intermediate water in the Northwestern Atlantic of 1.5–2.5°C (Fig S1) under a weakening of
665   the AMOC by 17–28%.

666   The water-isotope capability of iCESM can also help to further validate that our
667   sedimentary $\delta^{18}O$ records actually represent changes in temperature by investigating the
668   contribution of changes in $\delta^{18}O$ of seawater. The simulated water $\delta^{18}O$ enrichment of about
669   0.2–0.3‰ suggests a major increase in the proportion of saltier, $\delta^{18}O$-enriched water from the

670 Gulf Stream and ATSW (Fig 2). The heavier modelled $\delta^{18}O$ also discards potential effect

671 related to the injection of freshwater in the system. This seawater $\delta^{18}O$ enrichment could

672 influence our benthic $\delta^{18}O$ record in the opposite way than warming, which depletes the $\delta^{18}O$

673 recorded in carbonate. Therefore, the amplitude of our temperature reconstruction should be

674 considered as a conservative estimation. While a sensitivity experiment conducted with iCESM

675 (iPOP2-Trace) suggests that the $\delta^{18}O$ of carbonate at the MD99-2220 coring location might be

676 heavier because of change in pCO$_2$ (Zhang et al., 2017), the effect is also opposite to the signal

677 observed in our record.

678

679 **4. Oxygen isotopes as a record for temperature**

680 Oxygen isotopes in carbonate marine organisms vary with the temperature of

681 calcification and the $\delta^{18}O$ value of the water mass in which they calcify (Shackleton, 1974).

682 This counteracting effect has been previously investigated in Laurentian channel sediment

683 cores by comparing high-resolution benthic foraminifera $\delta^{18}O$ records to instrumental

684 temperature and salinity data (Thibodeau et al., 2010a). It was demonstrated that $\delta^{18}O$ in

685 benthic foraminifera underestimated the actual temperature increase (i.e., creating lighter $\delta^{18}O$)

686 because of the increased proportion of Atlantic Intermediate Slope Water (characterized by

687 high $\delta^{18}O$) in the Laurentian Channel. Thus, our $\delta^{18}O$ records from the St. Lawrence should be

688 considered as a conservative tool to reconstruct the Laurentian Channel bottom water

689 temperature, as the full temperature increase is not expressed. This signal was also observed in

690 the model results (Fig 2), which further support our hypothesis. The relatively rapid residence

691 time (about 7 years) and the isolation of the Laurentian channel bottom water from overlying

692 freshwater make it resilient to other potential local processes affecting $\delta^{18}O$ and thus

693 representative of the western North Atlantic slope waters entering the channel, irrespective of

694 the timescale (Gilbert et al., 2005). This is further illustrated by the absence of statistically

695 different changes in temperature and salinity along the same potential density from Cabot Strait

696 though the St. Lawrence Estuary between 1970 and 1990, highlighting the potential for these

697 cores to reflect the condition of the water entering the channel (Gilbert et al., 2005). Because

698 the temperature of the bottom is directly controlled by the proportion of Atlantic Intermediate

699 Slope Water entering the Laurentian channel, the $\delta^{18}O$ in benthic foraminifera can also be

700 considered a tracer of changes in the regional oceanography.

701

702   5. **Statistical analysis**

703   We investigated the similarity of the 20th century Laurentian channel bottom water

704   instrumental temperature, $\delta^{15}N$ of corals and the AMOC index (Caesar et al., 2018) and how

705   well $\delta^{18}O$ of core CR02-23 recorded these trends (Fig 3) using a spearman correlation (non-

706   parametric). We did not detrend the data, as we are mostly interested in how well the $\delta^{18}O$ of

707   core CR02-23 captures the general trend and we wanted to minimize the influence of potential

708   lead and lag due to sample resolution, bioturbation smoothing, and variable sedimentation

709   rates. Results suggest a high degree of similarity between CR02-23 $\delta^{18}O$ and instrumental

710   temperature ($r = -0.76$, $p < 0.005$), CR02-23 $\delta^{18}O$ and coral $\delta^{15}N$ ($r = 0.79$, $p < 0.005$), and

711   CR02-23 $\delta^{18}O$ and AMOC index ($r = 0.70$, $p < 0.0001$). We also observed a high correlation

712   between the AMOC index and instrumental temperature ($r = -0.55$, $p < 0.005$), and the coral

713    $\delta^{15}N$ ($r = 0.62$, $p < 0.005$). The coral $\delta^{15}N$ is also similar to the instrumental temperature ($r = -$

714   0.77, $p < 0.005$).

715   The 20th century values in core MD are significantly different when comparing them to

716   both the complete record (~700–1960), the pre-1600, and the 1600-1899 period ($p < 0.005$ for

717   both Kruskal-Wallis and one-way ANOVA). Using the same tests, we found that the 1600-

718   1899 period is not significantly different from the complete record, but it is significantly

719   different from the pre-1600 record ($p < 0.05$ for both Kruskal-Wallis and one-way ANOVA).

720   The means and the 95% confidence interval for each period can be seen in Fig S5.

721

722   Supplementary Figures

723   Figure 1. Modelled impact of a weakening of the AMOC on the temperature in the western
724   North Atlantic.

725   Figure 2. Budget analysis of the subsurface warming.

726   Figure 3. Updated age models for core piston core MD99-2220 and its box core AH00-2220
727   and box core CR02-23.

728   Figure 4. $\delta^{18}O$ from core MD99-2220 (red) and CR02-23 (pink) and $\delta^{15}N$ from Sherwood's
729   corals.

730   Figure 5. Means and confidence intervals (95%) of the different time periods in core MD99-
731   2220

732
733

734

735

736   **Figure S1. Modelled impact of a weakening of the AMOC on the temperature in the**

737   **western North Atlantic.** In the bottom panel we illustrate the modeled ocean temperature

738   changes over the Northwest Atlantic after 100 years of freshwater forcing in the iCESM and

739   UVic model. Depth-longitude section of ocean temperature in the upper 1,000 m of the western

740   North Atlantic at 45°N in the preindustrial control simulation (**a,b**) and the changes after 100-

741   year water hosing (**c,d**). We can observe the warming of the intermediate water of 2–2.5°C and

742   1–1.5°C next to the Laurentian channel entrance (dashed boxes) in the iCESM and UVic model,

743   respectively. Note that the magnitude of the freshwater forcing is 0.10 Sv in the iCESM and

744   0.05 Sv in the UVic model.

745
746
747
748
749
750
751
752
753
754
755
756
757
758
759
760
761
762
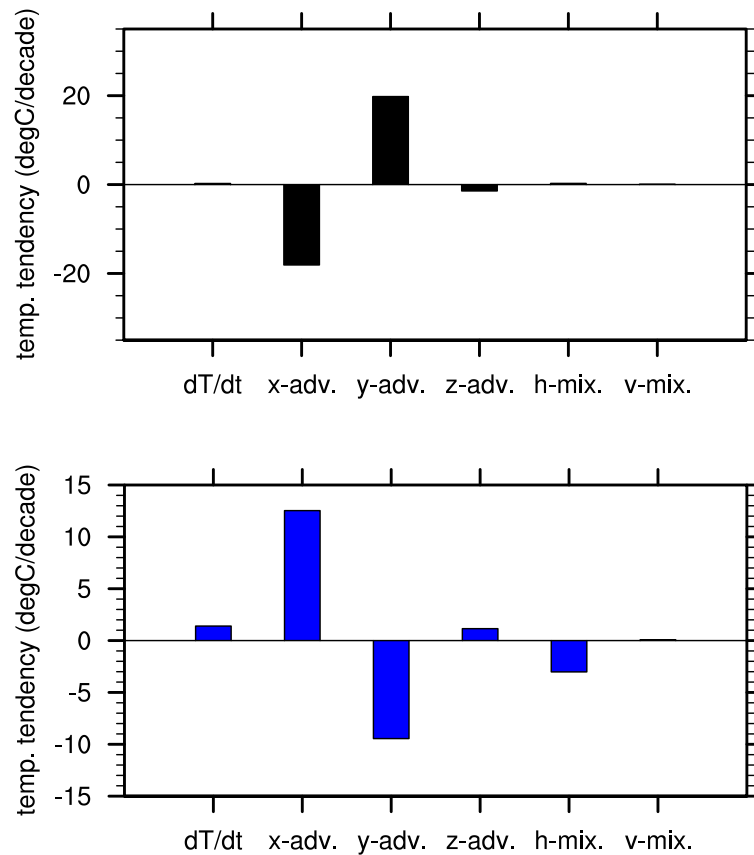763
764
765
766
767
768
769
770

Figure S2. Budget analysis of the subsurface warming. Terms in the temperature equation of the northwestern North Atlantic subsurface ocean (44–46°N, 300–320°E, 400m) in the preindustrial control simulation in iCESM (left; units: °C decade^{-1}). From left to right are: the temperature tendency, the zonal advection, the meridional advection, the vertical advection, the horizontal mixing and vertical mixing. Bottom panel shows the changes averaged between year 91 and 100 in the freshwater perturbation experiments. We note that the subsurface warming is dominantly caused by change in the zonal component of gyre circulations, which is coherent with a reorganization of the subsurface current suggested in Fig 1.
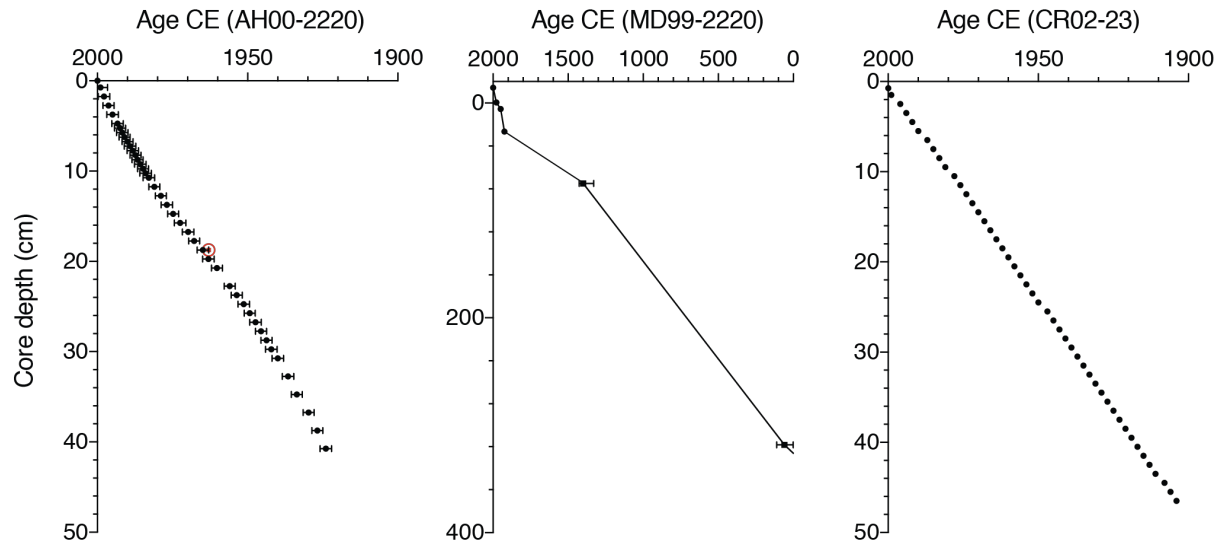
780

781

782
783

784 **Figure S3. Updated age models for core piston core MD99-2220 and its box core AH00-**

785 **2220 and box core CR02-23.** We updated the ^{210}Pb-derived age model for box cores AH00-

786 2220 and CR02-23 by using the constant rate supply model (Ghaleb, 2009; Sanchez-Cabeza &

787 Ruiz-Fernández, 2012), which estimate the age of each layer independently (i.e., the

788 sedimentation rate can vary in this model). Previous models have used a constant initial

789 concentration model, which implies a constant sedimentation rate. The precision (±1.8 years)

790 of the ^{210}Pb-derived age model for box core AH00-2220 was determined by comparing the

791 ^{210}Pb-derived age to the highest concentration of [137]Cs (1964.8), which is attributed to the peak

792 (red dot) of nuclear testing in 1963 (Left panel). The middle panel shows the composite age

793 model for piston core MD99-2220, which lost its top 14 cm in the coring process. The right

794 panel represents the ^{210}Pb-derived age model for box core CR02-23. Detailed data and

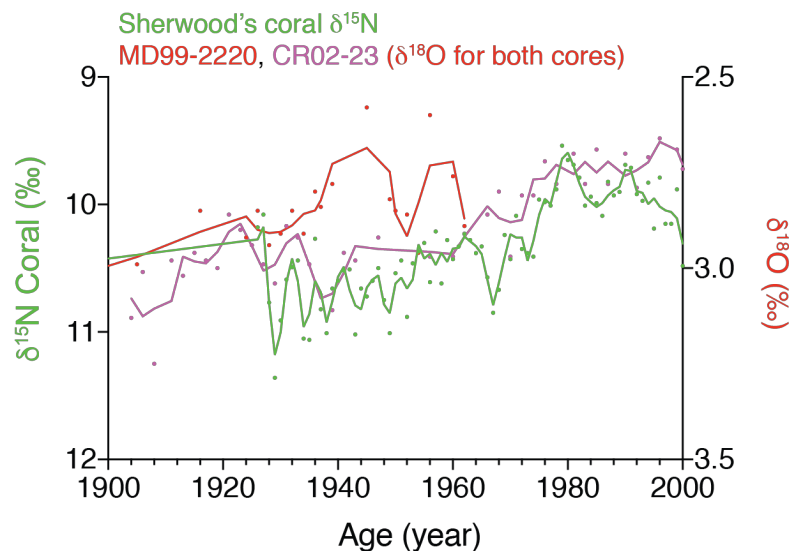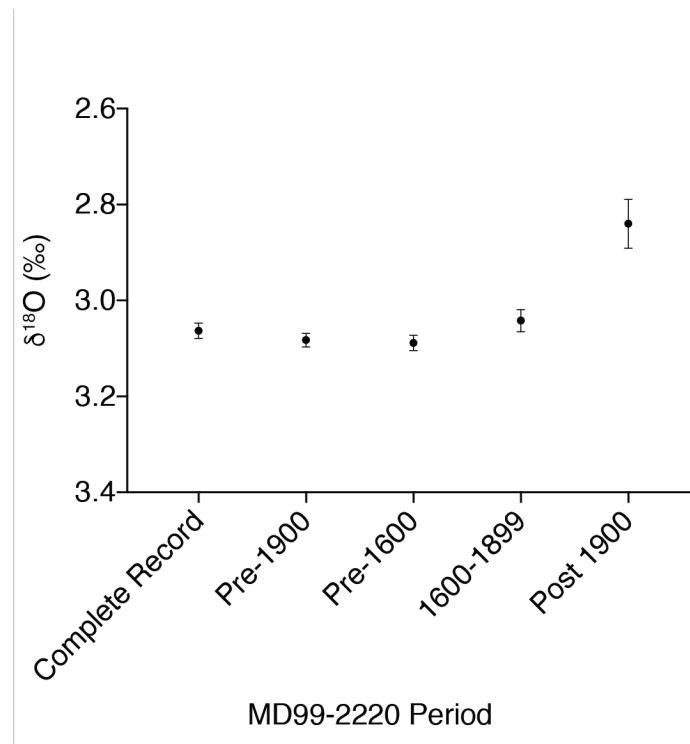795 calculation for the age models are available in the online data.

796
797

798
799
800 **Figure S4. δ^{18}O from core MD99-2220 (red) and CR02-23 (pink) and δ^{15}N from**

801 **Sherwood's corals.** The δ^{18}O at 1900 is 3‰ for MD99-2220 and 3.10‰ for CR02-23. The

802 lowest value is 2.6‰ for MD and 2.66‰ for CR. Thus, the amplitude of the change is

803 similar. There is a clear offset between the dating of the lowest value, which happen much

804 faster in core MD. Since we know the top of the core was lost during the piston coring of

805 MD, we rather not used this part of the core and focus our high-resolution analysis on the box

806 core CR that is well dated with ^{210}Pb

807
808

809

810

Figure S5. Means and confidence intervals (95%) of the different time periods in core MD99-2220. The post-1900 period is significantly different than any other period while the 1600-1899 period is significantly different than the pre-1600 period.

814
815